THE ASTROPHYSICAL JOURNAL, 502:428–436, 1998 July 20

A COMBINED MODEL FOR THE X-RAY TO GAMMA-RAY EMISSION OF CYGNUS X-1

IGOR V. MOSKALENKO,[1] WERNER COLLMAR, AND VOLKER SCHÖNFELDER
Max-Planck-Institut für extraterrestrische Physik, Postfach 1603, D-85740 Garching, Germany; imos@mpe.mpg.de; wec@mpe.mpg.de; vos@mpe.mpg.de
Received 1997 September 16; accepted 1998 March 2

ABSTRACT

We use recent data obtained by three (OSSE, BATSE, and COMPTEL) of four instruments on board the *Compton Gamma Ray Observatory* (*CGRO*) to construct a model of Cyg X-1 that describes its emission in a broad energy range, from soft X-rays to MeV γ-rays, self-consistently. The γ-ray emission is interpreted to be the result of Comptonization, bremsstrahlung, and positron annihilation in a hot, optically thin, and spatially extended region surrounding the whole accretion disk. For the X-ray emission, a standard corona-disk model is applied. We show that the Cyg X-1 spectrum accumulated by the *CGRO* instruments during a $\sim$4 year time period between 1991 and 1995, as well as the *HEAO 3* γ_1 and γ_2 spectra, can be well represented by our model. The derived parameters match the observational results obtained from X-ray measurements.

Subject headings: elementary particles — gamma rays: theory — plasmas — radiation mechanisms: nonthermal — scattering — stars: individual (Cyg X-1)

1. INTRODUCTION

One of the brightest sources in the low-energy γ-ray sky, Cyg X-1 has been extensively studied during the three decades since its discovery (Bowyer et al. 1965; for a review, see Oda 1977; Liang & Nolan 1984). It is a high-mass binary system (HDE 226868) with an orbital period of 5.6 days and consisting of a blue supergiant and, presumably, a black hole (BH) with a mass in excess of 5 $M_\odot$ (Dolan 1992). The separation of the two components is $\approx 4 \times 10^{12}$ cm (Beall et al. 1984). A periodicity of 294 days found in X-ray and optical light curves is thought to be related to precession of the accretion disk (Priedhorsky, Terrell, & Holt 1983; Kemp et al. 1983).

The X-ray flux of Cyg X-1 varies on all observed timescales down to a few milliseconds (e.g., Cui et al. 1997), but the average flux exhibits roughly a two-modal behavior. Most of the time Cyg X-1 stays in a so-called "low" state, where the soft X-ray luminosity (2–10 keV) is low. The low-state spectrum is hard and can be described by a power law with a photon index of $\sim$1.7 in the 10–150 keV energy band. There are occasional periods of "high"-state emission, in which the spectrum consists of a relatively stable, soft, blackbody component and a weak, variable, hard power-law component. The anticorrelation between the soft and hard X-ray components is remarkable (Liang & Nolan 1984) and is clearly seen during the transition phases between the two states.

Cyg X-1 is believed to be powered by accretion through an accretion disk. Its X-ray spectrum indicates the existence of a hot X-ray–emitting and a cold-reflecting gas. The soft blackbody component is thought to consist of thermal emission from an optically thick and cool accretion disk (Shakura & Sunyaev 1973; Pringle 1981; Bałucińska-Church et al. 1995). The hard X-ray part ($\gtrsim$10 keV) with a break at $\sim$150 keV has been attributed to thermal emission of the accreting matter Comptonized by a hot corona with temperature from tens to hundreds of keV (Bisnovatyi-Kogan & Blinnikov 1976; Sunyaev & Titarchuk 1980; Liang & Nolan 1984). A broad hump peaking at $\sim$20 keV (Done et al. 1992), an iron Kα emission line at $\sim$6.2 keV with an equivalent width $\sim$100 eV (Barr, White, & Page 1985; Kitamoto et al. 1990; see also Ebisawa et al. 1996 and references therein), and a strong iron K-edge (e.g., see Inoue 1989; Tanaka 1991; Ebisawa et al. 1992, 1996) have been interpreted as signatures of Compton reflection of hard X-rays off cold-accreting material.

In addition, there have also been sporadic reports of a hard spectral component extending into the MeV region. The most famous one was the so-called "MeV bump" observed at a 5 σ level during the *HEAO 3* mission (Ling et al. 1987). For a discussion of the pre–*Compton Gamma Ray Observatory* (*CGRO*) data and γ-ray emission mechanisms see, e.g., a review by Owens & McConnell (1992). The COMPTEL spectrum, accumulated over 15 weeks of real observation time during the 1991–1995 time period, shows significant emission out to several MeV (McConnell et al. 1997), which, however, always remained—by more than an order of magnitude—below the MeV bump reported from the *HEAO 3* mission.

The annihilation line search provided only tentative (1.9 σ) evidence for a weak 511 keV line with a flux of $(4.4 \pm 2.4) \times 10^{-4}$ photons cm^{-2} s^{-1} (Ling & Wheaton 1989). Recent OSSE observations (Phlips et al. 1996) resulted only in upper limits with values of $\leq 7 \times 10^{-5}$ cm^{-2} s^{-1} for a narrow 511 keV line and $\leq 2 \times 10^{-4}$ cm^{-2} s^{-1} for a broad feature at 511 keV.

Although an unified view for the X-ray spectra of BH candidates and their spectral states has yet to be constructed, the qualitative picture seems to be quite clear. Current popular models include an optically thick disk component, a hot Comptonizing region (e.g., Haardt et al. 1993; Gierliński et al. 1997), and/or an advection-dominated accretion flow (e.g., Abramowicz et al. 1995; Narayan & Yi 1995 and references therein). The spectral changes are probably governed by the mass accretion rate (e.g., Chen et al. 1995; Esin, McClintock, & Narayan 1997).

This picture, however, provides no explanation for the observed γ-ray emission (e.g., McConnell et al. 1997). The hard MeV tail cannot be explained by standard Compton models because they predict fluxes that are too small at MeV energies; thus, another mechanism is required. The

[1] Also, Institute for Nuclear Physics, M. V. Lomonosov Moscow State University, 119 899 Moscow, Russia.

models developed so far connect the γ-ray emission with a compact hot core (~ 400 keV or more) in the innermost part of the accretion disk, which emits via bremsstrahlung, Compton scattering, and annihilation (Liang & Dermer 1988; Skibo & Dermer 1995) or with π^0 production due to collisions of ions with nearly virial temperature (e.g., Kolykhalov & Sunyaev 1979; Jourdain & Roques 1994). Li, Kusunose, & Liang (1996) have shown that stochastic particle acceleration via wave-particle resonant interactions in plasmas (~ 100 keV) around the BH could provide a suprathermal electron population and is able to reproduce the hard-state MeV tail. The possibility of Comptonization in the relativistic gas inflow near the BH horizon has been discussed by Titarchuk & Zannias (1998).

We use the recent data obtained by three of four instruments aboard *CGRO* to construct a model of Cyg X-1, which describes its emission in a wide energy range, from soft X-rays to MeV γ-rays (Moskalenko, Collmar, & Schönfelder 1997). Instead of a compact (pair-dominated) γ-ray–emitting region, we consider an optically thin and spatially extended one surrounding the whole accretion disk. It produces γ-rays via Comptonization, bremsstrahlung, and positron annihilation. For the X-ray emission the corona-disk model is retained.

In § 2 we discuss the combined OSSE-BATSE-COMPTEL spectrum of Cyg X-1. Our model and the inferred results are described in §§ 3–4, and the implications are discussed in § 5. The applied formalism is given in the Appendices.

2. OBSERVATIONS

Since its launch in 1991, *CGRO* has observed Cyg X-1 several times. The time-averaged COMPTEL spectrum, based on all observations between the *CGRO* Phases 1 and 3 (1991 April–1994 November), is shown in Figure 1 (McConnell et al. 1997) together with the nearly contemporaneous spectrum derived from BATSE (Ling et al. 1997). The thick solid curve shows the best fit to the OSSE spectrum (0.06–1 MeV) for all observations between 1991 April and 1995 May (Phlips et al. 1996). The best-fit parameters

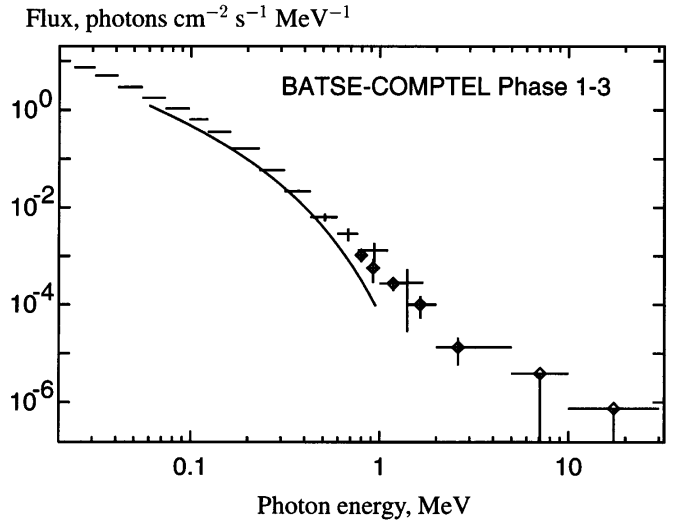

FIG. 1.—Average spectrum of Cyg X-1 (*diamonds*) based on all COMPTEL *CGRO* Phase 1–3 observations (McConnell et al. 1997). Crosses represent the almost contemporaneous BATSE data (Ling et al. 1997). The solid curve represents the best fit to the time-averaged OSSE spectrum containing 122 days of observation time (Phlips et al. 1996).

for a power-law model with an exponential cutoff are a power-law photon index of $\Gamma = 1.39$, a cutoff energy $E_c = 158$ keV, and a normalization intensity of 0.470 photons cm^{-2} s^{-1} MeV^{-1} at 0.1 MeV. The COMPTEL data provide evidence for a hard power-law tail extending up to at least 3 MeV.

Although the OSSE and BATSE spectra have similar shapes, their intensity normalizations are different by a factor of ~ 2 (Fig. 1). The discrepancy is largest at the highest energies, around 1 MeV. The COMPTEL measurements lie in between OSSE and BATSE. Although there is no way of deducing the exact spectral shape in this region, the total spectrum is probably smooth, without bumps, which is illustrated by the three individual spectra. Possible reasons for this discrepancy have been discussed by McConnell et al. (1997). For our further analyses we will use the combined BATSE-COMPTEL spectrum.

Table 1 lists the average luminosities of Cyg X-1 for various energy bands. The values are derived from the combined BATSE-COMPTEL spectrum assuming a source distance of 2.5 kpc. The total luminosity is between 1% and 10% of the Eddington luminosity,

$$L_{\rm Edd} \equiv 4\pi GM \frac{m_p c}{\sigma_{\rm T}} \approx 1.25 \times 10^{39} \text{ ergs s}^{-1} \left(\frac{M}{10\, M_\odot} \right), \quad (1)$$

where $\sigma_{\rm T}$ is the Thomson cross section.

3. THE MODEL

The existence of a compact, pair-dominated core around the BH in Cyg X-1 is unlikely in view of the *CGRO* observations. The signature of such a core would be a bump (Liang & Dermer 1988; Liang 1990) similar to the one reported by *HEAO 3*. However, no evidence for such a bump was detected by *CGRO* (Phlips et al. 1996; McConnell et al. 1997). In addition, the luminosity of Cyg X-1 above ~ 0.5 MeV, though small, would substantially exceed the Eddington luminosity for pairs, which is ~ 2000 times lower than that for a hydrogen plasma. On the other hand, the hard MeV tail observed by COMPTEL cannot be explained by Comptonization in a corona of $kT \sim 100$ keV, and therefore another mechanism is required.

Our study is an attempt to extend the "standard" disk-corona model, which has been shown to work quite well at X-ray energies (e.g., Gierliński et al. 1997; Dove et al. 1997), by including the processes of γ-ray emission. We investigate the proton-dominated, optically thin solution (Svensson 1984), $\Theta \equiv kT/m_e c^2 \lesssim 1$, where the γ-ray emission is attributed to a spatially extended cloud surrounding the whole accretion disk (Fig. 2), the outer corona, which emits via bremsstrahlung, Comptonization, and positron annihilation. We concentrate on the hard X-ray to γ-ray part of the spectrum, and thus we bring into consideration the aforementioned processes as well as Comptonization of the

TABLE 1

LUMINOSITY OF CYG X-1

Energy Band (MeV)	Luminosity (10^{36} ergs s^{-1})
≥ 0.02.....	26.0
0.02–0.2.....	20.5
0.2–1	4.8
≥ 1	0.6

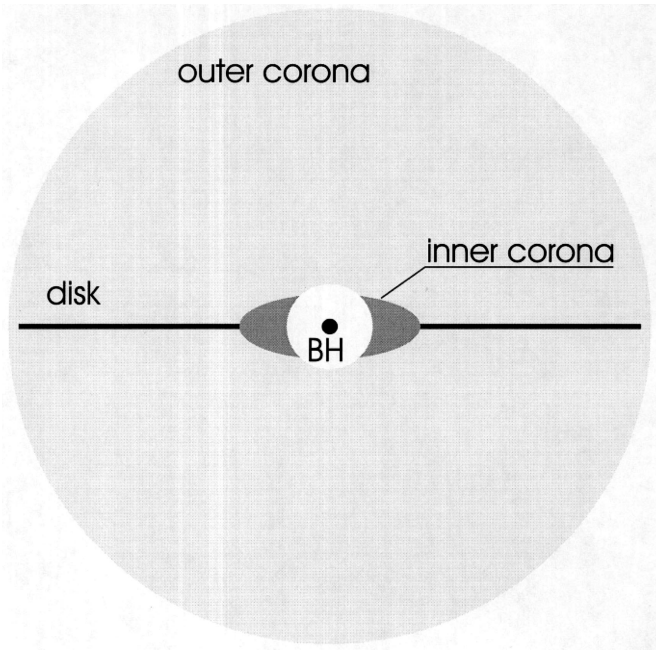

FIG. 2.—Schematic view illustrating the model

soft X-ray disk emission in the "standard" inner corona. The optical depth of the outer corona has to be small enough to avoid effective reprocessing of the emission from the disk and the inner corona. The soft X-rays consist of two components, the local blackbody emission from the disk plus the reflected spectrum. At energies above ≈ 30 keV, the former is negligible and the latter is only of minor importance. Therefore, we neglect both components at the moment and leave the detailed spectral modeling until the discrepancy in the intensity normalization of the OSSE and BATSE spectra has been resolved. However, the effective temperature of the soft excess is used in calculations of Comptonization in the inner and outer coronae, and the estimate of the total soft X-ray luminosity is provided to match the observed value.

Our idea is that the electrons in the outer corona (which is optically very thin) are relativistic. The heating mechanism is not specified, but people usually refer to stochastic acceleration (Li, Kusunose, & Liang 1996), MHD turbulence in the inner corona (Li & Miller 1997), and plasma instabilities in magnetized advection-dominated accretion flows (Bisnovatyi-Kogan & Lovelace 1997). These mechanisms are likely to heat mainly electrons and so can provide a population of energetic particles. We further show (see § 5) that the mean free path of these electrons in the outer corona is of the same order as its size. Because there is no mechanism to confine energetic electrons (and pairs if they exist) except for reasons of charge conservation, they can move freely inside the outer corona providing the same temperature for the whole plasma volume. Additionally, the electron cooling in a thermal plasma at low number density and small optical depth is not very efficient.

We do not consider the process of π^0 production in p-p collisions. Although it could be important at a few Schwarzschild radii (where the energy of protons is nearly virial), it is unimportant at tens to hundreds of Schwarzschild radii, which is the characteristic size of the outer corona. The protons in the accreting flow far from the BH horizon should be cold, since the gravitational forces are quite weak there, and thus the viscous heating in the disk is negligible. The energy transfer due to the Coulomb coupling with the hot electrons is also not efficient.

3.1. *The Fitting Parameters*

A set of eight fitting parameters was chosen: kT_i, τ_i, kT_o, and τ_o, the temperature and optical depth of the inner (i) and the outer (o) coronae, which are assumed to be spheres; $L^*_{\rm soft}$, the luminosity of the *disk* which is *effectively* Comptonized by the inner corona; $L_{\rm soft}$, the *total* effective soft X-ray luminosity of the central source illuminating the outer corona; R, the outer corona radius; and $Z = n_+/n_p$, the positron-to-proton ratio in it.

The formulae to calculate the bremsstrahlung, annihilation, and Comptonization emissivities are given in the Appendices. The accretion disk spectrum, which is further reprocessed by the inner and outer coronae, was taken to be monoenergetic with an energy $E_0 = 1.6kT_{bb}$ corresponding to the maximum of the Planck distribution, where $kT_{bb} = 0.13$ keV is the effective temperature of the soft excess (Bałucińska-Church et al. 1995).

The bremsstrahlung and annihilation photon fluxes from the outer corona are proportional to $R^3 n_i n_j$, where $n_{i,j}$ are the number densities of the plasma particles (see eqs. [A1] and [A3]). Thus, if the annihilation contributes significantly, there is a continuum of solutions given by the set of equations

$$R^3 n_- n_+ \equiv R^3 n_p^2 Z(1+Z) = \frac{R\tau_o^2 Z(1+Z)}{\sigma_{\rm T}^2 (1+2Z)^2} = \text{const}\ ,$$

$$\tau_o = \sigma_{\rm T} R n_p (1+2Z) = \text{const}\ , \qquad (2)$$

where kT_o is fixed, n_p is the proton number density and $Z(1+Z)/(1+2Z)^2$ varies slowly for $Z \gtrsim 0.5$ (therefore, the fitting procedure is not very sensitive to this parameter). If only a negligible positron fraction is present, the continuum of solutions is defined by

$$\tau_o = R n_p \sigma_{\rm T} = \text{const}\ , \qquad (3)$$

where kT_o is fixed, $R \le R_{\rm max}$, and $R_{\rm max}$ is fixed from the fitting procedure.

4. RESULTS

The observed spectra of Cyg X-1 are shown in Figures 3 and 4 together with our model calculations. The Comptonized spectrum from the outer corona is only shown up to 3 MeV because of two reasons: the measurements above consist of upper limits only, and up to this energy our approximation (see Appendix A, § A2) has been tested to agree reasonably with Monte Carlo simulations. The best-fit parameters of our model are listed in Table 2. Two sets of parameters with the same χ^2_ν are shown[2] for comparison, indicating that several solutions are possible. We consider the first one (I), however, to be more physical.

The average BATSE-COMPTEL spectrum probably corresponds to the "normal" (low) state of Cyg X-1. Only two components contribute: the Comptonized emission from the inner coronae and that from the outer coronae. Bremsstrahlung is of minor importance. By comparing set I

[2] The value of χ^2_ν cannot be used for the likelihood criterion estimates here, mainly because of the uncertainty in the relative normalization of the OSSE, BATSE, and COMPTEL data.

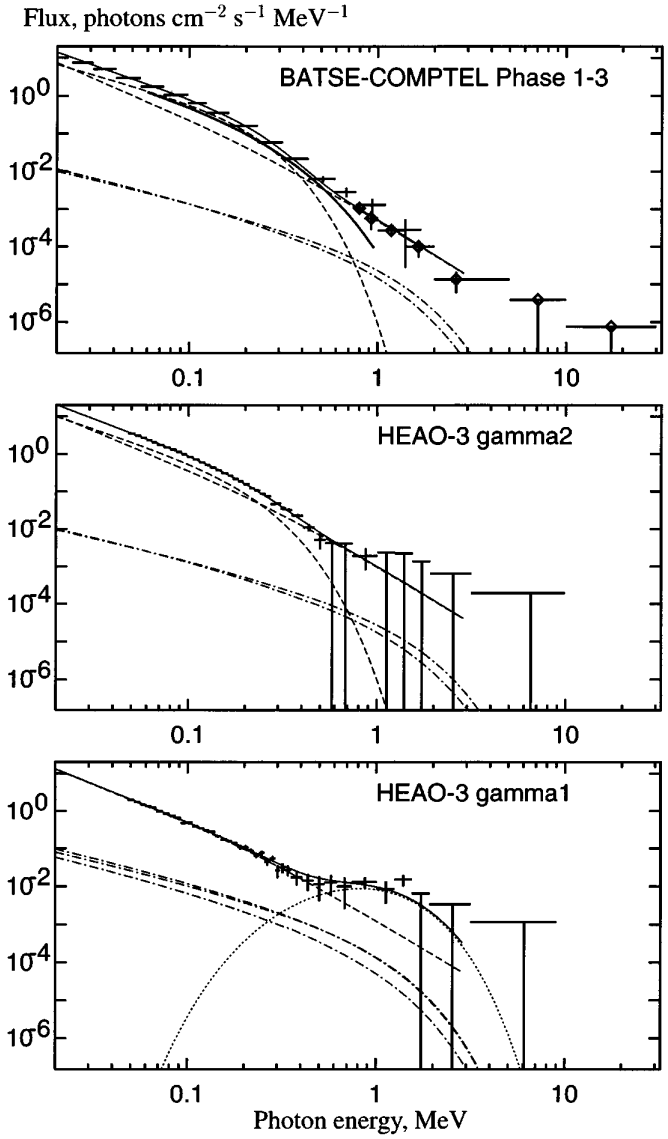

FIG. 3.—*Upper panel*: Calculated Cyg X-1 spectrum together with the data points, which are the same as in Fig. 1. *Central and lower panels: HEAO 3* γ_2 and γ_1 spectra (Ling et al. 1987). In all panels, the thin solid lines represent our model fitted for the parameter sets I. The individual spectral components are the annihilation line (*dotted line*), *e-e*, e^+-e^-, *e-p* bremsstrahlung (*dash-dotted line*), and the Comptonized spectra from the inner and outer coronae (*dashed lines*). The Comptonized spectra from the outer corona are shown up to 3 MeV, up to which the approximation used agrees with Monte Carlo simulations and also where significant data points are available.

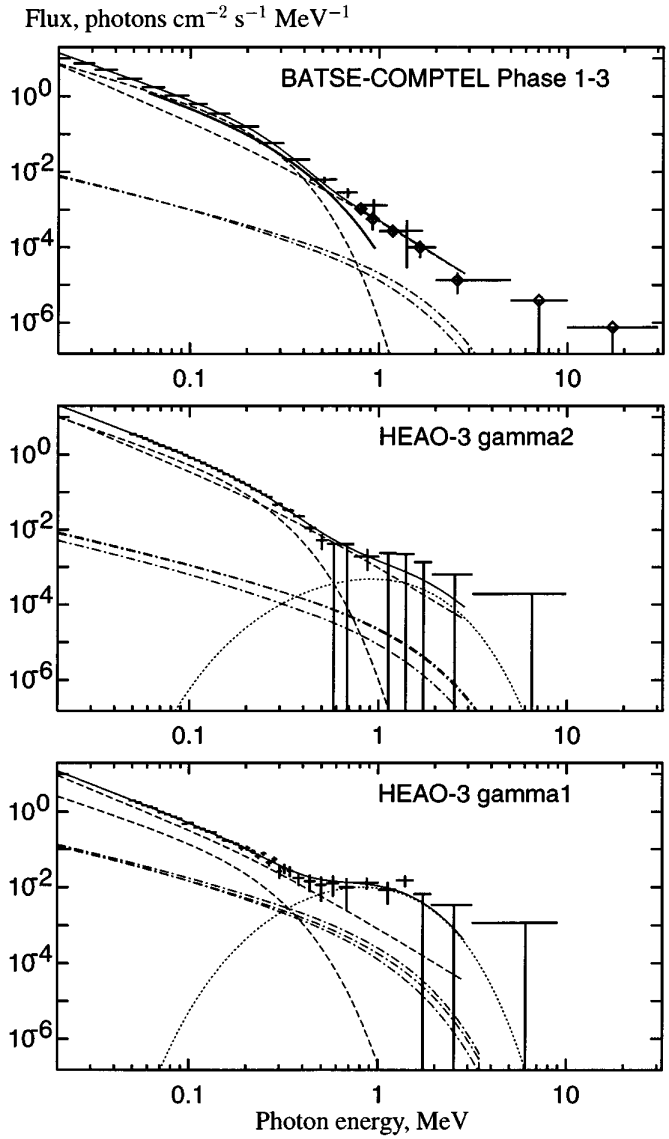

FIG. 4.—Same as in Fig. 3, but for parameter sets II (see Table 2)

and II, one can see that a smaller optical depth of the outer corona corresponds to a higher temperature. The parameters obtained for the *HEAO 3* γ_2 state are similar, although the spectral upper limits at high energies ($\gtrsim 1$ MeV) allow some positron fraction (set II).

The *HEAO 3* γ_1 "bump" spectrum has not been confirmed so far, but if true, it corresponds in our model to an outer corona size that is several times larger than in the "normal" state, when the inner corona is small or even absent (set I). A nonnegligible positron fraction (for R, n_p, Z dependence see eq. [2]) is too large to be produced in the optically thin outer corona (Svensson 1984). Therefore, we suggest a positron production mechanism (i.e., pair production in γ-γ, γ-particle, or particle-particle collisions), which might sometimes operate in the inner disk. The radiation pressure would necessarily cause a pair wind, which serves as energy input into the outer corona and thereby enlarging its radius. Note that matter outflows were found in many accreting binaries. At least two systems, 1E 1740.7−2942 and Nova Muscae, provide clear evidence for pair plasma streams (for a discussion see Moskalenko & Jourdain 1997a, 1997b).

A small disk luminosity of $L^*_{\rm soft} \approx 10^{36}$ ergs s^{-1}, which is Comptonized by the *inner* corona, probably implies a geometry where only the inner part of the disk is effectively covered by the corona, which means that most of the soft X-ray photons can escape and reach the observer. The covering factor is estimated to be ~ 0.18 by applying a value of 4.7×10^{36} ergs s^{-1} for the total observed luminosity of the soft excess (Bałucińska-Church et al. 1995, for a distance of 2.5 kpc). This value agrees well with a covering factor $\lesssim 0.2$ obtained by Dove et al. (1997) from self-consistent Monte Carlo modeling of the corona-disk structure. A slab (plane-parallel) corona-disk geometry is not capable of reproducing the observed broadband X-ray spectrum of Cyg X-1 (Gierliński et al. 1997; Dove et al. 1997).

TABLE 2

THE "BEST-FIT" MODEL PARAMETERS

PARAMETERS	CGRO PHASE 1–3		HEAO 3 γ_2-STATE		HEAO 3 γ_1-STATE	
	I	II	I	II	I[a]	II
Soft X-ray luminosity, L_{soft} (10^{36} ergs s^{-1})	9.0	8.0	10.6	10.7	9.8	7.9
i-Corona temperature, kT_i (keV)	76.7	79.7	95	94.9	...	93.0
i-Corona optical depth, τ_i	2.39	2.23	1.41	1.42	...	1.44
L^*_{soft}(10^{36} ergs s^{-1})	0.73	0.84	1.96	1.95	...	0.51
o-Corona temperature, kT_o (keV)	396	436	450	448	346	361
o-Corona optical depth, τ_o	0.06	0.05	0.056	0.056	0.12	0.10
o-Corona radius, R (10^8 cm)[b]	$\lesssim$100	$\lesssim$100	$\lesssim$100	150	391	812
Positron-to-proton ratio, Z[b]	0	0	0	1.0	1.0	0.5
Proton number density, n_p (10^{10} cm^{-3})[b]	$\gtrsim$900	$\gtrsim$750	$\gtrsim$840	187	154	93
Accretion disk radius, R_d (10^8 cm)	...	...	...	1	1	1
511 keV line flux, I_a (10^{-5} photons cm^{-2} s^{-1})[c]	0	0	0	0.18	0.15	0.04
χ^2_ν	4.0	3.9	1.4	1.4	0.9	0.9

[a] The inner corona is small or even absent.
[b] For R, n_p, Z dependence see eqs. (2) and (3).
[c] The narrow annihilation line flux from the disk (eq. [A4]) as calculated for the given R_d.

Such a picture is supported by X-ray observations. The OSSE correlation analysis of source temperature (defined from the thin thermal bremsstrahlung model) versus 45–140 keV intensity (Phlips et al. 1996) showed that the source temperature and the intensity vary only within a limited range: $\sim$130–170 keV and $\sim$0.07–0.12 photons cm^{-2} s^{-1}, with few low-temperature, low-amplitude exceptions. A similar behavior of the best-fit bremsstrahlung temperature versus hard X-ray luminosity (40–200 keV) has been found by Kuznetsov et al. (1997) from the analysis of the entire dataset of the Granat/SIGMA observations of Cyg X-1 collected between 1990 and 1994.

The soft X-ray (<10 keV) luminosity of Cyg X-1 is on the average $\sim 8.5 \times 10^{36}$ ergs s^{-1} (e.g., Liang & Nolan 1984; Ebisawa et al. 1996). During the *HEAO 3* γ_1 and γ_2 states it was even lower (Ling et al. 1987). Taking into account that for the hard X-ray photons the Comptonization efficiency in the hot plasma drops substantially (e.g., Hua & Titarchuk 1995) and the number of photons decreases as well, the values of $L_{soft} \approx 10^{37}$ ergs s^{-1} we obtain match the observational results.

No pairs are required to reproduce the spectrum of Cyg X-1 in its normal state. If one takes an annihilation line flux of $I_a \approx 4.4 \times 10^{-4}$ photons cm^{-2} s^{-1} (Ling & Wheaton 1989) in the γ_1 state, the accretion disk radius is estimated to be $R_d \sim 1.7 \times 10^9$ cm (eq. [A4], set I). The upper limit allowed by optical measurements is $R_d \approx 6 \times 10^9$ cm ($M/10$ $M_\odot$) (Liang & Nolan 1984), while the effective radius of the soft X-ray–emitting region of the disk is $\sim 4.6 \times 10^7$ cm (Bałucińska-Church et al. 1995).

Our calculations show that the presented model is consistent with the available observations of the Cyg X-1 system and is able to reproduce the observed spectra well. A more detailed study, however, would require a solution of the discrepancy in the intensity normalization between the OSSE and BATSE data and further Monte Carlo modeling.

5. DISCUSSION

We have calculated the radiation from Cyg X-1 self-consistently assuming that the hot, optically thin outer corona exists. A mechanism of its maintenance was not specified in our model (so it is not *totally* self-consistent), but the energy required to maintain such a corona is quite small and could be provided by a turbulent mechanism, stochastic particle acceleration, and/or diffusion of high-energy electrons from the inner disk (e.g., see Li, Kusunose, & Liang 1996 and references therein). A relevant example is the solar corona of $\sim 10^6$ K (although its energetic contents is low), compared to 6000 K of the Sun's effective temperature; but a direct scaling to a BH is not appropriate here. In this section we discuss the physical conditions in the outer corona—i.e., diffusion of electrons and the cooling mechanisms—while we do not touch its origin.

To treat the diffusion of energetic electrons in the outer corona, we consider the *transport* cross section for *e-e* scattering. This (1) allows us to exclude unimportant scattering at small angles dominating in Coulomb interactions and (2) provides us with a correct estimate of the typical cross section, since the *e-p* collisions in a hot plasma are of minor importance compared to *e-e* collisions.

The transport cross section σ_{tr} (see Appendix) for electrons in a hydrogen plasma of $\Theta = 0.2$, 0.6, 0.8, and 1.0 is shown in Figure 5. Although the value of σ_{tr} for particles with a Lorentz factor $\gamma \sim 2$ is much larger than the Thomson cross section, the corresponding mean free path

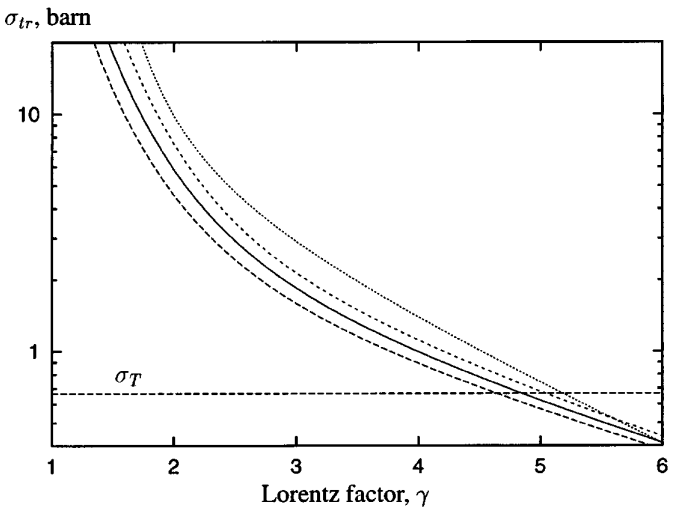

FIG. 5.—Transport cross section for electrons in a hydrogen plasma vs. the Lorentz factor of a particle. The individual lines correspond to the plasma temperatures (*from top to bottom*): $\Theta = 0.2$, 0.6, 0.8, 1.0. For comparison the Thomson cross section σ_T is also shown.

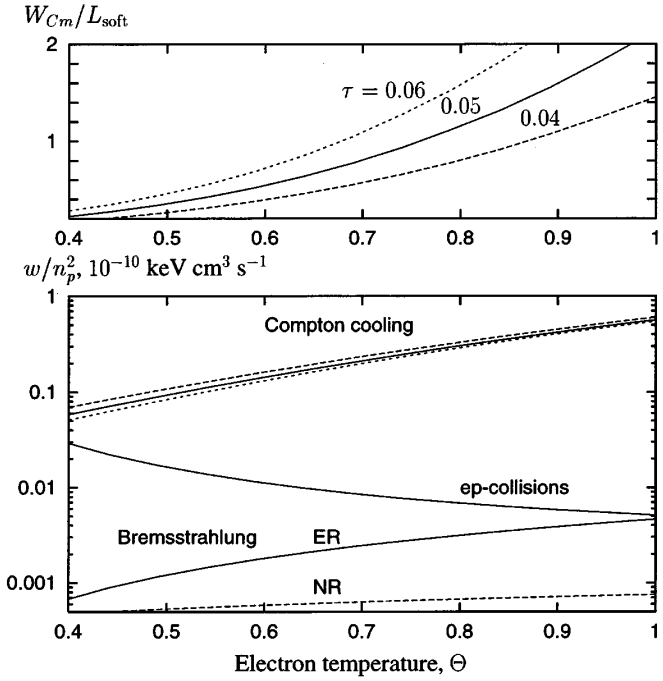

FIG. 6.—*Upper panel:* Total cooling rate due to the Compton scattering as function of the plasma temperature for several values of the optical depth (eq. [B4]). *Lower panel:* Cooling rates due to the electron bremsstrahlung $w_{ee} + w_{ep}$ (ER, NR) and Coulomb coupling with cold protons vs. plasma temperature ($Z = 0$; see Appendix). For the Compton scattering shown are the *average* cooling rates calculated for $R = 10^{10}$ cm, where the line styles and the optical depths correspond to these in the upper panel.

of electrons is close to the radius of the outer corona. This allows electrons to pass freely and therefore provides the same temperature for the whole plasma volume. Positrons, if produced somewhere, can also homogeneously fill the plasma volume. The annihilation timescale is given by (Svensson 1982)

$$t_a = \frac{1}{\pi r_e^2 c n_-} [1 + 2\Theta^2 \ln^{-1}(1.12\Theta + 1.3)] ,$$

$$t_a(\Theta \sim 1) \approx 400 \text{ s} \left(\frac{10^{12} \text{ cm}^{-3}}{n_-} \right) . \quad (4)$$

For the parameters listed in Table 2, t_a is of the order of hundreds of seconds.

The relevant cooling rates for electrons in a pure hydrogen plasma $Z = 0$ (see Appendix) are shown in Figure 6 (*lower panel*). The rates are divided by n_p^2; the Coulomb logarithm was taken as a constant of $\ln \Lambda = 20$. For comparison we show the *average* Compton energy losses per unit volume (divided by n_p^2), $w_{Cm} n_p^{-2} = W_{Cm} n_p^{-2} \times 3/(4\pi R^3) = W_{Cm} \times 3\ \sigma_T^2/(4\pi R \tau_o^2)$ (see eq. [3]), calculated for $L_{soft} = 10^{37}$ ergs s^{-1}, $\tau_o = 0.04$, 0.05, 0.06, and $R = 10^{10}$ cm. Clearly the average Comptonization losses (for τ_o fixed) depend on the radius of the outer corona and, for $\Theta \gtrsim 0.4$ and the parameters adopted, substantially dominate bremsstrahlung losses and losses due to the Coulomb coupling with cold protons. On the other hand, their total value is not too high, of the order of L_{soft} (*upper panel*), which is about 10%–20% of the total luminosity.

The average value of the Compton energy losses of an electron in the outer corona can be estimated as $dE/dt = W_{Cm}/N$, where $N = 4\pi\tau_o R^2/3\ \sigma_T$ is the total number of electrons in the outer corona. Taking the corresponding numerical values (Table 2), $W_{Cm} \approx L_{soft} \sim 10^{37}$ ergs s^{-1}, $\tau_o \sim 0.5$, $R = 10^{10}$ cm, one can obtain $dE/dt \approx 200$ keV s^{-1}. The appropriate timescale for an electron of $\gamma \sim 2$ is a few seconds, which is long compared to the $R/c \lesssim 1$ s the particle needs to cross the outer corona.

6. CONCLUSION

The data obtained recently by the *CGRO* instruments allow us to construct a model of Cyg X-1 that describes its emission from soft X-rays to MeV γ-rays self-consistently. This model is based on the suggestion that the γ-ray–emitting region is a hot, optically thin, spatially extended, proton-dominated cloud, the outer corona. The emission mechanisms are bremsstrahlung, Comptonization, and positron annihilation. For X-rays, a standard corona-disk model is applied.

The *CGRO* spectrum of Cyg X-1 accumulated over a $\sim$4 year period between 1991 and 1995, as well as the *HEAO 3* γ_1 and γ_2 spectra can be well represented by our model. The derived parameters also match the basic results of the X-ray observations. A fine-tuning of the model would require further Monte Carlo simulations and more accurate spectral measurements. In this respect, the solution of the discrepancy between the OSSE and BATSE normalizations would be of particular importance.

We thank the referee for useful comments. Discussions with R. Narayan, L. Titarchuk, and M. Gilfanov are greatly acknowledged. We are particularly grateful to M. McConnell for providing us with the combined spectra of Cyg X-1 prior to publication, and E. Churazov for Monte Carlo simulations of Comptonization in $\Theta \sim 1$, $\tau \approx 0.1$–0.05 plasma.

APPENDIX A

RADIATION FROM A THERMAL PLASMA

For a thermal plasma consisting of electrons, positrons, and protons at mildly relativistic temperatures ($kT \lesssim m_e c^2$), the main radiation processes are bremsstrahlung, electron-positron annihilation, and Compton scattering.

A1. BREMSSTRAHLUNG

The bremsstrahlung emissivities, the number of photons emitted per unit time, per unit volume, and per unit energy interval, can be represented by the form

$$S_{ij}(\varepsilon, kT) \propto n_i n_j \frac{e^{-\varepsilon/\Theta}}{\varepsilon} g_{ij}(\varepsilon, kT) , \tag{A1}$$

where $\varepsilon = E/m_e c^2$ is the dimensionless photon energy, $\Theta = kT/m_e c^2$ is the dimensionless plasma temperature, and $n_{i,j}$ with $i = (e^-, e^+)$, $j = (e^-, e^+, p)$ are the corresponding number densities. Accurate numerical fits for the Gaunt factors $g_{ee}(\varepsilon, kT)$ and $g_{e^+e^-}(\varepsilon, kT)$ in an appropriate energy range have been given by Stepney & Guilbert (1983) and Haug (1987), respectively. The *e-p* bremsstrahlung emissivity can be calculated by the one fold integration (e.g., see Stepney & Guilbert 1983). The approximations of the Gaunt factors $g_{ij}(\varepsilon, kT)$ have also been constructed by Skibo et al. (1995).

A2. COMPTONIZATION

To calculate the effect of Compton scattering in a medium of $kT \sim 100$ keV, we follow the model by Sunyaev & Titarchuk (1980) with corrections made by Titarchuk (1994) and Hua & Titarchuk (1995). The total number of photons emerging from the plasma cloud per unit energy interval and per unit time is given by

$$F(E, kT) = \frac{F_\nu(x, x_0) L_{\rm soft}}{E E_0} , \qquad x_0 \ll 1 , \qquad x_0 \ll x , \tag{A2}$$

where $x \equiv E/kT$, $x_0 \equiv E_0/kT$, E is the photon energy, E_0 is the energy of soft photons injected into the plasma, $L_{\rm soft}$ is the luminosity of the soft photon source, and $F_\nu(x, x_0)$ is the emergent spectrum represented by the Green's function (Hua & Titarchuk 1995).

The results of the Hua & Titarchuk (1995) model are generally in a good agreement with Monte Carlo simulations except at high temperatures, $\Theta \sim 1$, and small optical depth, $\tau \sim 0.1$–0.05 (Skibo et al. 1995). However, it still provides the correct spectral index. We found that the disagreement is mainly due to the steeper tail and the overall normalization, which is overestimated by the model. A simple power law with an exponential cutoff, $\propto (E_0/E)^{\alpha+1}(1 - e^{-kT/E})$, where α is determined by the transcendental equation (Titarchuk & Lyubarskij 1995), gives a reasonable agreement with simulations up to ~ 3 MeV. The chosen normalization provides the correct value of the amplification factor (see eq. [B4]).

A3. ANNIHILATION

The emissivity of a thermal plasma due to the electron-positron annihilation is (Dermer 1984)

$$S_a(\varepsilon, kT) = \frac{n_- n_+ c}{kT K_2^2(1/\Theta)} e^{-(2x^2+1)/2x\Theta} \int_1^\infty d\gamma_r (\gamma_r - 1) e^{-\gamma_r/2x\Theta} \sigma_a(\gamma_r) , \tag{A3}$$

where K_n is the modified Bessel function of the second kind and of order n, γ_r is the relative Lorentz factor of the colliding particles (invariant), and $\sigma_a(\gamma_r)$ is the annihilation cross section (Jauch & Rohrlich 1976).

The near-Earth intensity of the narrow annihilation line from the disk plane can be estimated by the assumption that all positrons that hit the disk annihilate in it (two annihilation photons per positron):

$$I_a \simeq \frac{n_+ c}{4} \frac{R_d^2}{D^2} \cos i_d , \tag{A4}$$

where n_+ is the number density of positrons in the outer corona and $\frac{1}{4} n_+ c$ is the flux density toward the disk surface, R_d is the disk radius, $D = 2.5$ kpc is the distance, and i_d is the inclination angle of the disk plane ($i_d \approx 40°$; Liang & Nolan 1984).

APPENDIX B

COOLING OF ELECTRONS

The electron cooling in a thermal plasma at low number density and small optical depth is not very effective. The main channels are bremsstrahlung, Comptonization, and Coulomb interactions with ions (mainly protons).

B1. BREMSSTRAHLUNG

For a pure hydrogen plasma the *e-p* bremsstrahlung luminosity dominates the *e-e* bremsstrahlung luminosity in the nonrelativistic limit, while at relativistic energies, $\Theta \gtrsim 0.5$, the *e-e* bremsstrahlung dominates. The total energy emitted per *unit volume* of plasma electrons by *e-p* plus e^+-e^- bremsstrahlung in the nonrelativistic limit, $\Theta \ll 1$, is

$$w_{ep}^{\rm NR} + w_{e^+e^-}^{\rm NR} \approx \frac{128}{3\pi^{1/2}} \alpha_f r_e^2 m_e c^3 n_p^2 \sqrt{\Theta} \left[\frac{1}{2^{3/2}} (1 + 2Z) + Z(1 + Z) \right] \tag{B1}$$

(Haug 1985), where $\alpha_f = 1/137$ is the fine-structure constant, and r_e is the classical electron radius. The total energy emitted by *e-e* plus e^+-e^- bremsstrahlung at the extreme-relativistic energies, $\Theta \gtrsim 1$, is given by

$$w_{ee}^{\rm ER} = 24 \alpha_f r_e^2 m_e c^3 n_p^2 (1 + 2Z)^2 \Theta [\ln(2\Theta) - 0.5772 + 5/4] \tag{B2}$$

(Alexanian 1968; Haug 1985), and that for *e-p* bremsstrahlung is

$$w_{ep}^{\mathrm{ER}} = 12\alpha_f r_e^2 m_e c^3 n_p^2 (1 + 2Z)\Theta[\ln(2\Theta) - 0.5772 + 3/2] \tag{B3}$$

(von Stickforth 1961; Haug 1975).

B2. COMPTON COOLING

An expression for the *total* energy losses of a plasma volume via Comptonization has been given by Dermer, Liang, & Canfield (1991):

$$W_{\mathrm{Cm}} = L_{\mathrm{soft}} \frac{P(A-1)}{1-PA}\left[1 - \left(\frac{x_0}{3}\right)^{-1-\ln P/\ln A}\right], \tag{B4}$$

where

$$P = 1 - e^{-\tau}, \qquad A = 1 + 4\Theta \frac{K_3(1/\Theta)}{K_2(1/\Theta)}, \tag{B5}$$

$x_0 \equiv E_0/kT$ (see eq. [A2]), and L_{soft} is the luminosity of the soft photon source. For $\tau \ll 1$ and $x_0 \ll 1$, equation (B4) is almost exact. The luminosity enhancement factor is given by $\eta \equiv L/L_{\mathrm{soft}} = 1 + W_{\mathrm{Cm}}/L_{\mathrm{soft}}$.

B3. COULOMB COUPLING WITH PROTONS

Stepney & Guilbert (1983) derived a general expression for the rate of energy transfer between populations of protons and electrons with Maxwellian distributions:

$$w_{\mathrm{Cl}} = 4\frac{m_e}{m_p}\pi r_e^2 c n_p^2 (1 + 2Z)\ln\Lambda \frac{kT_e - kT_p}{K_2(1/\Theta_e)K_2(1/\Theta_p)}\left[2K_0\left(\frac{\Theta_e + \Theta_p}{\Theta_e\Theta_p}\right) + \frac{2(\Theta_e + \Theta_p)^2 + 1}{\Theta_e + \Theta_p} K_1\left(\frac{\Theta_e + \Theta_p}{\Theta_e\Theta_p}\right)\right], \tag{B6}$$

where $\ln\Lambda$ is the Coulomb logarithm, $\Theta_e = kT_e/m_e c^2$, and $\Theta_p = kT_p/m_p c^2$ are the dimensionless electron and proton temperatures. The expression is symmetrical with respect to the electron and proton temperatures. In the limit of cold protons, $\Theta_p \to 0$, equation (B6) reduces to

$$w_{\mathrm{Cl}} = 4\frac{m_e^2}{m_p}\pi r_e^2 c^3 n_p^2 (1 + 2Z)\ln\Lambda \frac{2\Theta_e^2 + 2\Theta_e + 1}{K_2(1/\Theta_e)}. \tag{B7}$$

APPENDIX C

TRANSPORT CROSS SECTION

Scattering at very small angles dominates in the Coulomb cross section, which reflects the long-range nature of the Coulomb interaction. However, for the diffusion process in plasma, small scattering angles are not very important. Additionally the *e-p* collisions are of minor importance compared to *e-e* collisions. We therefore restrict ourselves by considering the transport cross section only for *e-e* scattering, which provides us with an estimate on typical values of the relevant cross sections.

The transport cross section for a test electron is defined by

$$\sigma_{\mathrm{tr}}(\gamma_1) = \int d^3p_2 \frac{\sqrt{\gamma_r^2 - 1}}{\gamma_1\gamma_2} f(p_2) \int d\Omega(1 - \cos\theta)\frac{d\sigma}{d\Omega} = \int d^3p_2 \frac{\sqrt{\gamma_r^2 - 1}}{\gamma_1\gamma_2} f(p_2) \int d\Omega^*(1 - \cos\theta)\frac{d\sigma^*}{d\Omega^*}, \tag{C1}$$

where β_1, γ_1 are the dimensionless speed and the Lorentz factor of the test particle, $f(p_2)$ is the Maxwell-Boltzmann distribution, $p_2 = \gamma_2\beta_2$ is the momentum of the plasma particles, $d\sigma/d\Omega$ is the differential cross section of the Coulomb scattering (Jauch & Rohrlich 1976), and the asterisk marks the center-of-mass system (CMS) variables. The scattering angle, expressed in CMS variables, is $\cos\theta = (\beta_c + \cos\theta^*)/(1 + \beta_c\cos\theta^*)$, where $\beta_c, \gamma_c = (\gamma_1 + \gamma_2)/[2(\gamma_r + 1)]^{1/2}$ are the speed and Lorentz factor of the CMS relative to the laboratory system. Changing to the integration variables γ_2 and γ_r, we obtain

$$\sigma_{\mathrm{tr}}(\gamma_1, \Theta) = \frac{1}{2\beta_1\gamma_1^2\Theta K_2(1/\Theta)}\int_1^\infty d\gamma_r(\gamma_r^2 - 1)^{1/2}\int_{\gamma^-}^{\gamma^+} d\gamma_2\,\tilde{\sigma}_{\mathrm{tr}}(\gamma_r, \gamma_c)e^{-\gamma_2/\Theta}, \tag{C2}$$

where $\gamma^{\pm} = \gamma_1\gamma_r(1 \pm \beta_1\beta_r)$, and

$$\tilde{\sigma}_{\mathrm{tr}}(\gamma_r, \gamma_c) = \int_{\cos\theta_M^*}^{\cos\theta_L^*} d(\cos\theta^*)\left(1 - \frac{\beta_c + \cos\theta^*}{1 + \beta_c\cos\theta^*}\right)\frac{d\sigma^*}{d(\cos\theta^*)} \tag{C3}$$

is the transport cross section for scattering angles θ^* greater than the limiting angle $\theta_L^* \to 0$, where $\theta_M^* = \pi/2$ for Møller scattering and $\theta_M^* = \pi$ for Bhabha scattering.

For Møller scattering, the expression is

$$\tilde{\sigma}_{\rm tr}(\gamma_r, \gamma_c) = \frac{4\pi r_e^2 \gamma_r^2}{(\gamma_r - 1)^2(\gamma_r + 1)} \left[(4\gamma_c^2 - 1) \ln\left(\frac{1+\beta_c}{2}\right) + \frac{2(1-\beta_c)}{1+\beta_c} (\ln\Lambda + \ln\sqrt{2}) + 1 \right] + \frac{1}{\gamma_r + 1} \left[\left(\frac{1}{\beta_c^2} - 5\right) \ln(1+\beta_c) - \frac{1}{\beta_c} + 4\ln 2 + 1 \right]. \quad \text{(C4)}$$

The mean free path of a test electron in a thermal plasma would be

$$\lambda(\gamma_1; \Theta) = \frac{\beta_1}{n_- \sigma_{\rm tr}(\gamma_1; \Theta)}. \quad \text{(C5)}$$

REFERENCES

Abramowicz, M. A., et al. 1995, ApJ, 438, L37
Alexanian, M. 1968, Phys. Rev., 165, 253
Bałucińska-Church, M., Belloni, T., Church, M. J., & Hasinger, G. 1995, A&A, 302, L5
Barr, P., White, N., & Page, C. G. 1985, MNRAS, 216, 65P
Beall, J. H., Knight, F. K., Smith, H. A., & Wood, K. S. 1984, ApJ, 284, 745
Bisnovatyi-Kogan, G. S., & Blinnikov, S. I. 1976, Soviet Astron. Lett., 2, 191
Bisnovatyi-Kogan, G. S., & Lovelace, R. V. E. 1997, ApJ, 486, L43
Bowyer, S., Byram, E. T., Chubb, T. A., & Friedman, M. 1965, Science, 147, 394
Chen, X., et al. 1995, ApJ, 443, L61
Cui, W., Zhang, S. N., Focke, W., & Swank, J. H. 1997, ApJ, 484, 383
Dermer, C. D. 1984, ApJ, 280, 328
Dermer, C. D., Liang, E. P., & Canfield, E. 1991, ApJ, 369, 410
Dolan, J. F. 1992, ApJ, 384, 249
Done, C., Mulchaey, J. S., Mushotzky, R. F., & Arnaud, K. A. 1992, ApJ, 395, 275
Dove, J. B., Wilms, J., Maisack, M., & Begelman, M. C. 1997, ApJ, 487, 759
Ebisawa, K., et al. 1992, in Frontiers of X-Ray Astronomy, ed. Y. Tanaka and K. Koyama (Tokyo: Univ. Acad. Press), 301
———. 1996, ApJ, 467, 419
Esin, A. A., McClintock, J. E., & Narayan, R. 1997, ApJ, 489, 867
Gierliński, M., et al. 1997, MNRAS, 288, 958
Haardt, F., Done, C., Matt, G., & Fabian, A. C. 1993, ApJ, 411, L95
Haug, E. 1975, Z. Naturforsch., 30a, 1546
———. 1985, A&A, 148, 386
———. 1987, A&A, 178, 292
Hua, X.-M., & Titarchuk, L. 1995, ApJ, 449, 188
Inoue, H. 1989, in 23d ESLAB Symp. 2, Two Topics in X-Ray Astronomy (Noordwijk: ESA), 783
Jauch, J., & Rohrlich, F. 1976, The Theory of Photons and Electrons (New York: Springer)
Jourdain, E., & Roques, J. P. 1994, ApJ, 426, L11
Kemp, J. C., et al. 1983, ApJ, 271, L65
Kitamoto, S., et al. 1990, PASJ, 42, 85
Kolykhalov, P. I., & Sunyaev, R. A. 1979, Soviet Astron., 23, 189
Kuznetsov, S., et al. 1997, MNRAS, 292, 651
Li, H., Kusunose, M., & Liang, E. P. 1996, ApJ, 460, L29
Li, H., & Miller, J. A. 1997, ApJ, 478, L67
Liang, E. P. 1990, A&A, 227, 447
Liang, E. P., & Dermer, C. D. 1988, ApJ, 325, L39
Liang, E. P., & Nolan, P. L. 1984, Space Sci. Rev. E, 38, 353
Ling, J. C., Mahoney, W. A., Wheaton, Wm. A., & Jacobson, A. S. 1987, ApJ, 321, L117
Ling, J. C., & Wheaton, Wm. A. 1989, ApJ, 343, L57
Ling, J. C., et al. 1997, ApJS, 484, 375
McConnell, M., et al. 1997, in AIP Conf. Proc. 410, Fourth Compton Symposium, ed. C. D. Dermer, M. S. Strickman, & J. D. Kurfess (New York: AIP), 829
Moskalenko, I. V., Collmar, W., & Schönfelder, V. 1997, in AIP Conf. Proc. 410, Fourth Compton Symposium, ed. C. D. Dermer, M. S. Strickman, & J. D. Kurfess (New York: AIP), 863
Moskalenko, I. V., & Jourdain, E. 1997a, in AIP Conf. Proc. 410, Fourth Compton Symposium, ed. C. D. Dermer, M. S. Strickman, & J. D. Kurfess (New York: AIP), 881
———. 1997b, A&A, 325, 401
Narayan, R., & Yi, I. 1995, ApJ, 452, 710
Oda, M. 1977, Space Sci. Rev., 20, 757
Owens, A., & McConnell, M. L. 1992, Comments Astrophys., 16, 205
Phlips, B. F., et al. 1996, ApJ, 465, 907
Priedhorsky, W., Terrell, J., & Holt, S. S. 1983, ApJ, 270, 233
Pringle, J. E. 1981, ARA&A, 19, 137
Shakura, N. I., & Sunyaev, R. A. 1973, A&A, 24, 337
Skibo, J. G., & Dermer, C. D. 1995, ApJ, 455, L25
Skibo, J. G., Dermer, C. D., Ramaty, R., & McKinley, J. M. 1995, ApJ, 446, 86
Stepney, S., & Guilbert, P. W. 1983, MNRAS, 204, 1269
Sunyaev, R. A., & Titarchuk, L. G. 1980, A&A, 86, 121
Svensson, R. 1982, ApJ, 258, 335
———. 1984, MNRAS, 209, 175
Tanaka, Y. 1991, Lecture Notes in Physics 385, Iron Line Diagnostics in X-Ray Sources, ed. A. Treves (Berlin: Springer), 98
Titarchuk, L. G. 1994, ApJ, 434, 570
Titarchuk, L., & Lyubarskij, Yu. 1995, ApJ, 450, 876
Titarchuk, L. G., & Zannias, T., 1998, ApJ, 493, 863
von Stickforth, J. 1961, Z. Phys., 164, 1

Note added in proof.—Recently, the discrepancy between the OSSE and BATSE spectra of Cyg X-1 in the hard state has been largely resolved by excluding from the averaging procedure those viewing periods for which OSSE measured a very low hard X-ray flux (M. McConnell et al., in preparation [1998]). While the BATSE and COMPTEL spectra remain essentially unchanged, the OSSE spectrum rose in flux and is now consistent with the average BATSE spectrum.